Nature Methods

Magnetic torque tweezers: measuring torsional stiffness in DNA and RecA-DNA filaments

Jan Lipfert, Jacob W J Kerssemakers, Tessa Jager & Nynke H Dekker

Supplementary Figure 1	Stability and resulution of the bead tracking in *x, y,* and *z*.
Supplementary Figure 2	Schematic of the angular tracking algorithm.
Supplementary Figure 3	Errors in angular tracking from position localization errors.
Supplementary Figure 4	Histograms of rotation angles obtained from bead tracking.
Supplementary Figure 5	Torsional trap stiffness as a function of force.
Supplementary Figure 6	Twist curve measurement with conventional magnetic tweezers.
Supplementary Figure 7	Analysis of angular fluctuations in the MTT.
Supplementary Figure 8	Measurement scheme to determine the torsional response of DNA.
Supplementary Figure 9	Torque measurements for dsDNA at varying stretching forces.
Supplementary Figure 10	Force-extension behavior of dsDNA.
Supplementary Figure 11	Rotation-extension behavior of dsDNA.
Supplementary Figure 12	Comparison of values for the effective twist persistence length of DNA determined by different methods.
Supplementary Figure 13	Force-extension measurements for RecA-DNA heteroduplex filaments.
Supplementary Figure 14	Torque response of a RecA filament at F = 3.5 pN.
Supplementary Figure 15	Partial disassembly of RecA filament determined from its rotation-extension response.
Supplementary Figure 16	Schematic of the magnetic assembly for the MTT.

Note: Supplementary Software is available on the Nature Methods website.

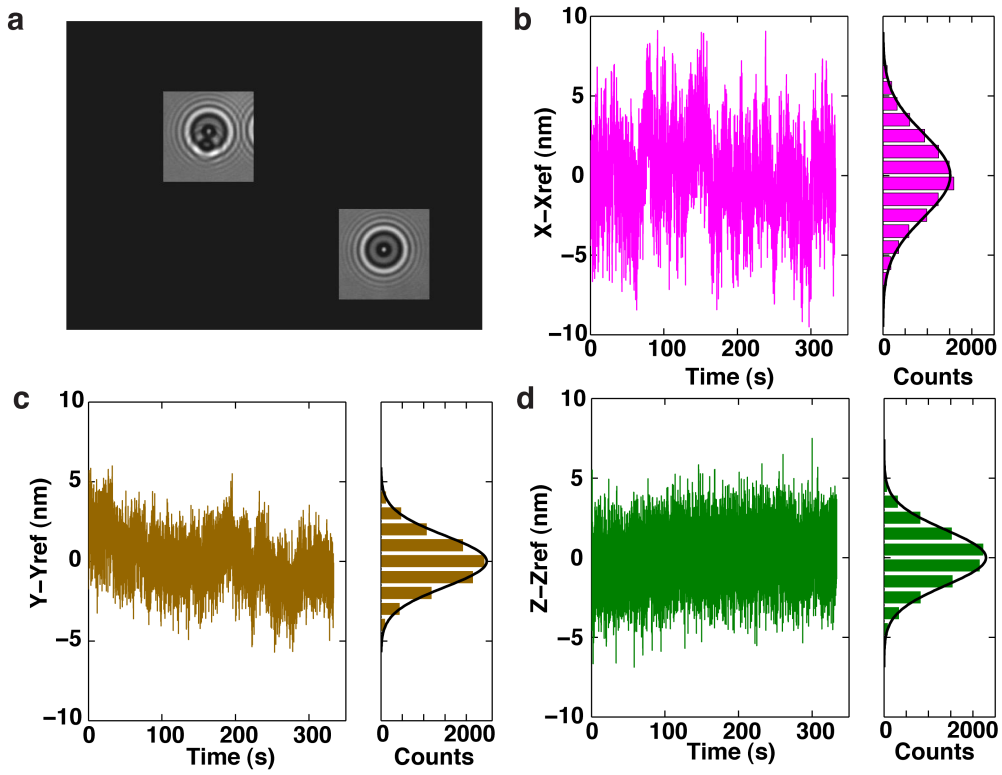

Supplementary Figure 1. Stability and resolution of the bead tracking in x, y, and z. To test the position resolution and stability of our bead tracking algorithm, a 1.4 μm radius magnetic and a 1.5 μm radius reference bead that are both unspecifically stuck to the flow cell surface are tracked from analysis of the CCD images. Similar to the situation for the measurements of tethered beads, the magnetic bead carries a 0.5 μm marker bead. The bead with the fiducial marker is treated as the "signal bead", the other stuck bead is used as a reference bead. To correct for mechanical drift, the reference bead position is subtracted from the "signal bead" position. (a) CCD image of the stuck beads. (b) Time trace and histogram of the x position, after subtracting the reference bead position. The standard deviation of the distribution of x positions is $\sigma(x) = 2.63$ nm. (c) Time trace and histogram of the y position, after subtracting the reference bead position. The standard deviation of the distribution of y positions is $\sigma(y) = 1.61$ nm. (d) Time trace and histogram of the z position, after subtracting the reference bead position. The standard deviation of the distribution of z positions is $\sigma(z) = 1.74$ nm.

Nature Methods: doi:10.1038/nmeth.1520

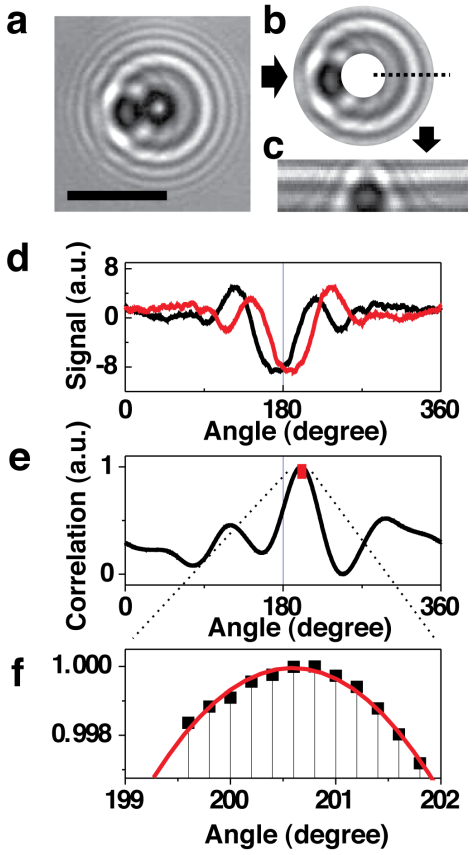

Supplementary Figure 2. Schematic of the angular tracking algorithm. (a) Defocused CCD image of a 1.4 μm radius bead with a smaller 0.5 μm radius fiducial marker bead. The scale bar corresponds to 7 μm. (b) Selection of a radial section containing the asymmetry induced by the smaller marker bead. (c) Polar transfomation of the image shown in (b), as described in the section "Rotational Tracking by Video Microscopy" in the Supplementary Information. (d) Angular signature (black curve) obtained from radially averaging the image in (a), and its own mirror (red curve). (e) Cross-correlation of the angular signature and its mirror image. The correlation image has a prominent maximum indicating the symmetry shift. (f) Sub-pixel fitting step to determine the angular position. A selection around the maximum of the correlation curve in (e) is used for an parabolic fit to yield an angular position at sub-pixel resolution.

Nature Methods: doi:10.1038/nmeth.1520

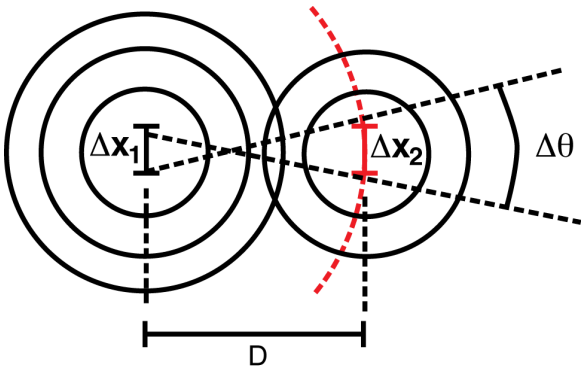

Supplementary Figure 3. Simple geometric model to illustrate how errors in angular tracking arise from position localization errors. In general, if we consider two reference positions spaced a distance D apart that can be localized with a position accuracy in x (or y) of Δx_1 or Δx_2, respectively, the limit on angular accuracy imposed by the tracking accuracy in x and y is approximately

$$\Delta\theta \approx \frac{\sqrt{\Delta x_1^2 + \Delta x_2^2}}{D}$$

Certainly, other additional sources of error like the inability to separate the diffraction pattern of the main bead from the tracking of the marker bead or the lack of a pronounced assymmetry in the image can further decrease the angular resolution. For our system of a 1.4 μm radius main bead with a 0.5 μm radius fiducial marker bead, we have D $\approx$ 1.9 μm. Assuming a position localization error of $\approx$ 2 nm (Supplementary Fig. 1), we expect a limit on the angular resolution from the x and y uncertainty alone of $\approx 0.1^\circ$, close to what we observe for the tracking of surface attached beads, indicating that our tracking algorithm performs close to the lower limit set by the x and y accuracy.

Nature Methods: doi:10.1038/nmeth.1520

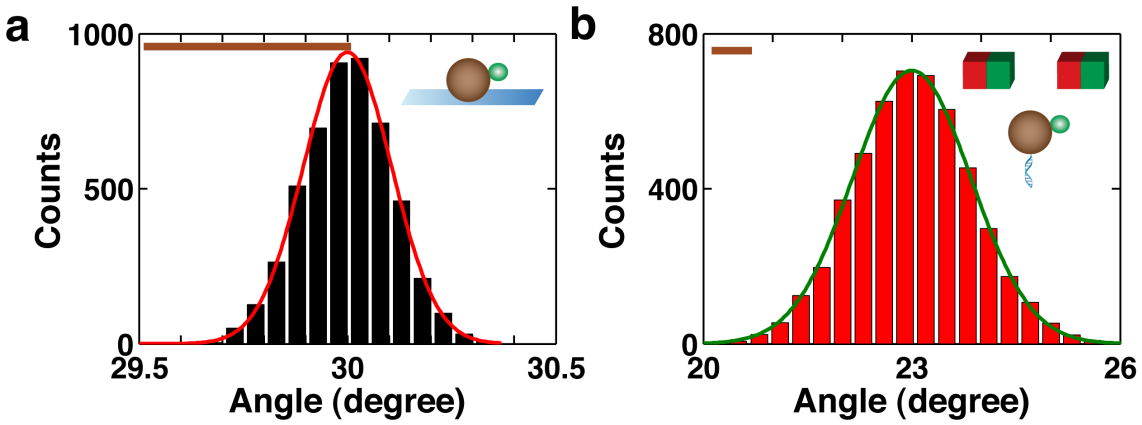

Supplementary Figure 4. Close up of the histograms of rotation angles obtained from tracking of magnetic beads. The histograms correspond to the same traces as shown in Fig. 1g of the main text. (a) Data for a bead non-specificially stuck to the surface (black histogram). The red line is a Gaussian fit with $\sigma = 0.10°$. (b) Histogram for a DNA tethered bead held in conventional magnetic tweezers (red histogram). The green line is a Gaussian fit with $\sigma = 0.85°$. The stretching force is 3.5 pN in both cases. For ease of comparison, the brown scale bar in the upper left corner indicates 0.5° in both panels.

Nature Methods: doi:10.1038/nmeth.1520

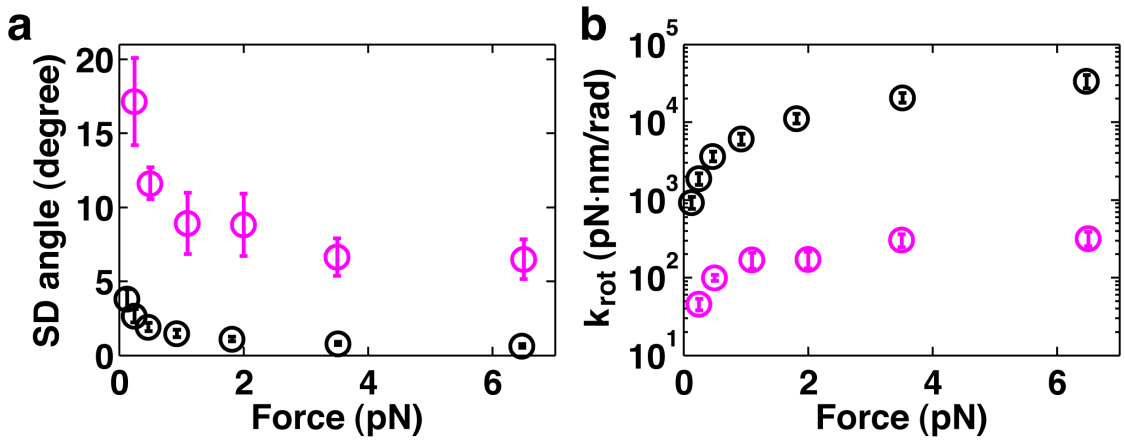

Supplementary Figure 5. Torsional trap stiffness as a function of force. (a) Standard deviation of the angular fluctuations as a functions of force for the MTT magnet geometry (magenta) and for conventional MT (black). Symbols correspond to the mean and standard deviation of at least six independent measurements for each force for the MTT measurements and of at least three independent measurements for the conventional MT data. (b) Torsional stiffness k_{rot} as a function of stretching force computed from the data in panel (a) using Equation 1 (main text). The MTT data shown are obtained from measurements using independent beads at the different forces. Control measurements with the same bead at different forces give the same result, within experimental error (not shown). It is apparent that for all forces studied the trap stiffness for the conventional MT set up is approximately two orders of magnitude higher than for the MTT magnet configuration. Details of the MTT magnet geometry are described in the "Magnets for Magnetic Torque Tweezers" section in the Supplementary Methods. For the conventional MT, we employed a pair of magnets in horizontal geometry, with a 1 mm gap and an iron yoke described in detail in Lipfert *et al.*[1]. Our results for conventional magnetic tweezers can be compared to the indirect measurements of the torsional stiffness obtained from analysis of the z-fluctuations by Klaue and Seidel[2]. Klaue and Seidel find values for k_{rot} in the range of 20-50 $\cdot 10^3$ pN·nm/rad for the force range explored in our measurements. While a direct and quantitative comparison is precluded by the fact that Klaue and Seidel employed M280 beads while our measurements used M270 beads, their values are in order-of-magnitude agreement with the measurements presented in panel (b).

Nature Methods: doi:10.1038/nmeth.1520

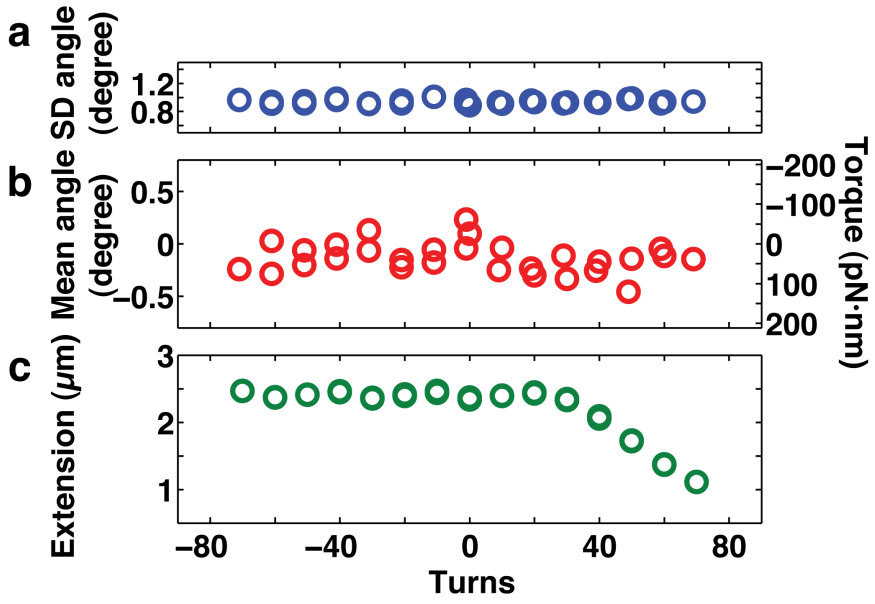

Supplementary Figure 6. Twist curve measurement with conventional MT. A twist curve similar to Supplementary Fig. 8a was recorded using a conventional MT geometry at a force of ≈ 2 pN. For each plateau the mean and standard deviation of the angular fluctuations as well as the tether extension were determined. (a) Standard deviations of the angular fluctuations as a function of rotations. The angular fluctuations consistently exhibit a standard deviation of slightly less than 1°, corresponding to a trap stiffness of ≈ 15,000 pN·nm/rad. (b) The mean of the angle signal as a function of magnet rotations. It is apparent that the mean angle of the plateaus essentially shows no systematic trend, but exhibits random scatter with a magnitude of ≈ 0.1-0.2°. The standard deviation taken over all the mean values is 0.14°. Due to the high torsional trap stiffness, this random scatter corresponds to large torque excursions, on the order of ≈ 50 pN·nm (right axis in panel (b)). (c) Tether extension as a function of magnet rotations. Multiple data points for each number of turns correspond to repeat measurements for the same magnet rotation setting. The data were recorded starting at 0 turns, going out to 70 turns, scanning to -70, and returning to 0 all in steps of 10 turns, using the 7.9 kbp DNA construct in PBS buffer. The conventional magnet geometry employed consists of a pair of magnets in horizontal geometry, with a 1 mm gap and an iron yoke described in detail in Lipfert *et al.*[1].

Nature Methods: doi:10.1038/nmeth.1520

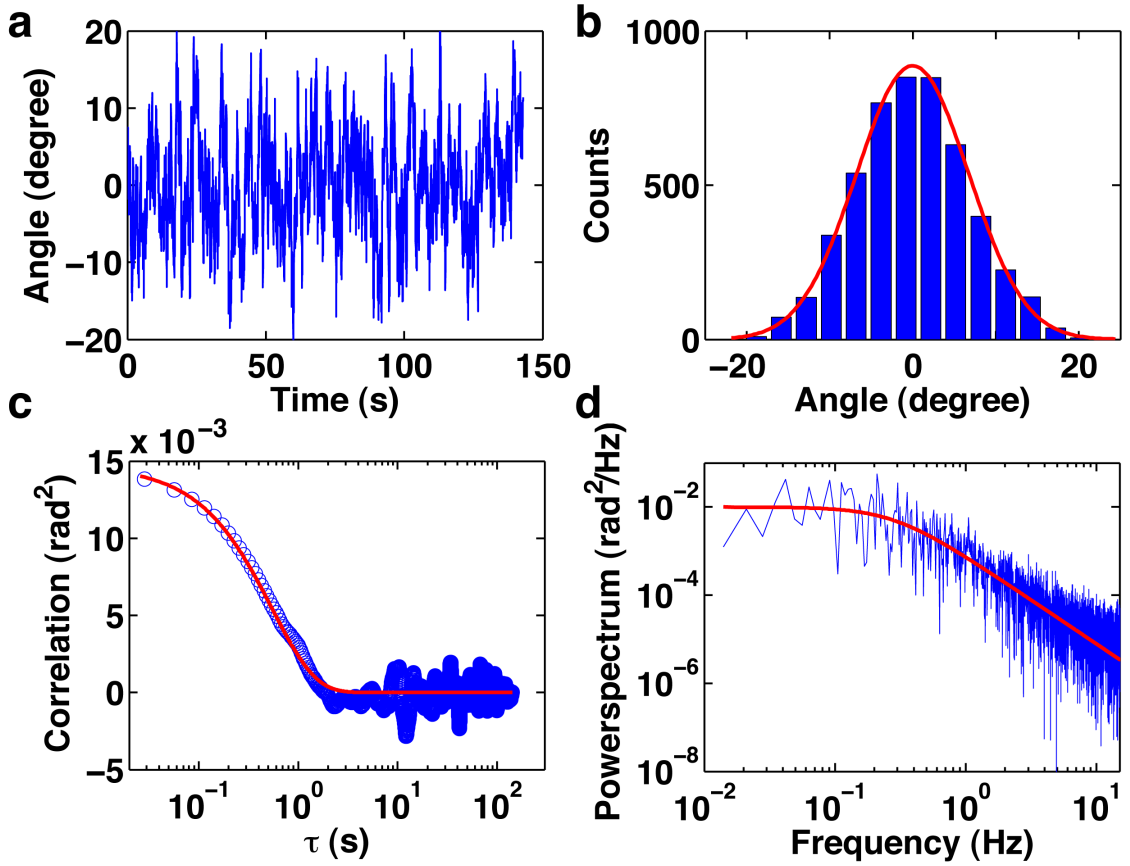

Supplementary Figure 7. Analysis of the rotational trap via rotational fluctuations and friction in the MTT. (a) Representative angle trace, shown as angle vs. time, for a bead tethered in the MTT set up at a stretching force of 3.5 pN. (b) Histogram of the angle fluctuations shown in panel (a). The red line is a Gaussian fit to the data, yielding a standard deviation of $\sigma = 6.75° = 0.12$ rad. This standard deviation corresponds via Equation 1 of the main text to a trap stiffness $k_{\mathrm{rot}} = 295$ pN·nm/rad (see also Supplementary Fig. 5). (c) Analysis of the temporal autocorrelation. The blue symbols show temporal correlation of the data shown in panel (a) as a function of the correlation time τ. The red line is a fit of an exponential function derived below in the "Derivation of the temporal correlation function" section. (d) Power spectrum of the rotational fluctuations shown in panel (a). The red line is a fit of a Lorentzian function described below in the "Analysis of the power spectrum" section.

Derivation of the temporal correlation function. We define the temporal correlation

Nature Methods: doi:10.1038/nmeth.1520

function as

$$Corr(\tau) = \langle \theta(t)\theta(t+\tau) \rangle = \lim_{T\to\infty} \frac{1}{T} \int_0^T \theta(t)\theta(t+\tau)dt \tag{1}$$

where we have chosen the coordinate system of the angular coordinate θ w.l.o.g. such that the mean of the angle is zero, i.e. $\langle\theta\rangle = \theta_0 = 0$. By definition, the autocorrelation for zero time is equal to the variance of the angle; by the equipartition theorem the variance of the angle is equal to the absolute temperature divided by the trap stiffness (Equation 1 of the main text)

$$Corr(\tau = 0) = \langle \theta(t)^2 \rangle = \mathrm{Var}(\theta) = \frac{k_B T}{k_{\mathrm{rot}}} \tag{2}$$

For a trapped particle undergoing Brownian fluctuations in the rotational trap the equation of motion is a Langevin equation. Since we are in the overdamped limit, we can neglect the inertial term and write

$$\gamma_{\mathrm{rot}} \frac{d\theta}{dt} + k_{\mathrm{rot}}\theta(T) = F_{\mathrm{therm}}(t) \tag{3}$$

where γ_{rot} is the (rotational) friction coefficient, k_{rot} is again the rotational trap stiffness, and $F_{\mathrm{therm}}(t)$ is the Langevin force from random collisions of the particle with the solvent. Since the collisions are uncorrelated on the time scale of our measurement $F_{\mathrm{therm}}(t) \sim \delta(t)$. Inserting the expression for $\theta(t)$ into the definition of the correlation function, the integral in the definition of $Corr(\tau)$ averages to zero for $\tau > 0$ as the Brownian fluctuations are uncorrelated; therefore $Corr(\tau)$ satisfies

$$\gamma_{\mathrm{rot}} \frac{dCorr(\tau)}{d\tau} + k_{\mathrm{rot}} Corr(\tau) = 0 \tag{4}$$

which has the solution

$$Corr(\tau) = Corr(\tau = 0) \exp\left(-\frac{k_{\mathrm{rot}}}{\gamma_{\mathrm{rot}}}\tau\right) = \frac{k_B T}{k_{\mathrm{rot}}} \exp\left(-\frac{k_{\mathrm{rot}}}{\gamma_{\mathrm{rot}}}\tau\right) \tag{5}$$

We can define the critical angular (rotation) frequency of the system

$$\omega_c = \frac{k_{\mathrm{rot}}}{\gamma_{\mathrm{rot}}} \tag{6}$$

or equivalently the characteristic time $\tau_c = \omega_c^{-1}$. From a fit of an exponential function (red line) to the data (blue symbols), we obtain $k_{\mathrm{rot}} = 295$ pN·nm/rad and $\gamma_{\mathrm{rot}} = 163$ pN·nm·s, corresponding to a characteristic time of $\tau_c = 0.55$ s.

Rotational friction coefficient for the bead construct in the MTT. The friction coefficient obtained from the fit to the temporal correlation data can be compared to the

Nature Methods: doi:10.1038/nmeth.1520

expected value calculated for the MTT bead construct geometry, which consist of the magnetic bead with a radius of 1.4 μm and a (in some cases, possibly a few) marker bead(s) with a radius of 0.5 μm attached to the magnetic bead. A perfect sphere of radius R rotating around its center has a rotational friction coefficient given by[3]

$$\gamma_{\mathrm{rot}}^{\mathrm{sphere,c}} = 8\pi\eta R^3 \tag{7}$$

where η is the fluids viscosity, $\eta \approx 10^{-3}$ kg/(m·s) for our aqueous buffer. For $R = 1.4$ μm, we find $\gamma_{\mathrm{rot}}^{\mathrm{sphere,c}} \approx 70$ pN·nm·s. This value provides an order of magnitude estimate for the expected friction coefficient of our MTT, however, this estimate is too low, as several additional factors will increase the friction coefficient. These factors are i) rotation about an axis that does not go through the center of the sphere, ii) the influence of the attached marker bead(s), and iii) the influence of the surface. While it is difficult to exactly determine the geometry of the MTT construct and to quantify all of these factors, we provide a semi-quantitative discussion of these effects below.

If the bead does not rotate around an axis through its center, but on a circle with radius R_{circ} instead, the friction coefficient is given by

$$\gamma_{\mathrm{rot}}^{\mathrm{sphere}} = 8\pi\eta R^3 + 6\pi\eta R R_{\mathrm{circ}}^2 \tag{8}$$

For the case where bead rotates about an axis through its equator, such that $R_{\mathrm{circ}} = R$, the friction coefficient simplifies to $14\pi\eta R^3$, a 75% increase compared to the case of rotation around a central axis.

We can estimate the influence of an attached marker bead on the overall drag coefficient if we assume that its contribution is approximately independent of the main bead. A 0.5 μm radius marker bead attached at the equator of the a main bead that rotates about an axis through its center rotates on a circle of radius $R_{\mathrm{circ}} = 1.4$ μm + 0.5 μm and experiences a rotational friction coefficient of ≈ 40 pN·nm·s. The hydrodynamic coupling of the two beads will tend to decrease the contribution of the smaller bead. Similarly, the contribution will be smaller for a bead not attached at the equator. In contrast, the contribution of the smaller bead will potentially be increased if the rotation is about an off-center axis.

Finally, the proximity of the surface will tend to increase the friction coefficient. For translational motion this effect is known as Faxén's law[4]. For rotational motion, no analytical solution is known, but the effective friction coefficient will also be increased if the rotating sphere is within a distance of about R from the surface[5]. In our experiments, the bead is ≈ 2 - 2.5 μm from the surface, which is less than $2R$ and suggests that the surface effects should be modest, but non-negligible.

In summary, the above semi-quantitative arguments suggest that the friction coefficient for the combined MTT bead assembly is in the range of 100-200 pN·nm·s, in good agreement with the value determined from the fit in panel (c). Similar values for the friction coefficient were observed for other beads and we found the fitted friction coefficients to be

Nature Methods: doi:10.1038/nmeth.1520

approximately independent of stretching force (not shown).

Analysis of the power spectrum Applying the treatment of Brownian fluctuations in a potential well[6] to rotational motion[7], it can be shown that the power spectrum of the angular fluctuations has the form of a Lorentzian

$$S(f) = \frac{A}{1 + \left(\frac{f}{f_c}\right)^2} \tag{9}$$

where f_c is the critical or corner frequency related to the critical angular frequency by $\omega_c = 2\pi f_c$. From a fit of the Lorentzian function (panel (d), red line) we find $f_c = 0.28$ Hz, in good agreement with the value determined from the correlation analysis $1/(2\pi\tau_c) = 0.29$ Hz.

Nature Methods: doi:10.1038/nmeth.1520

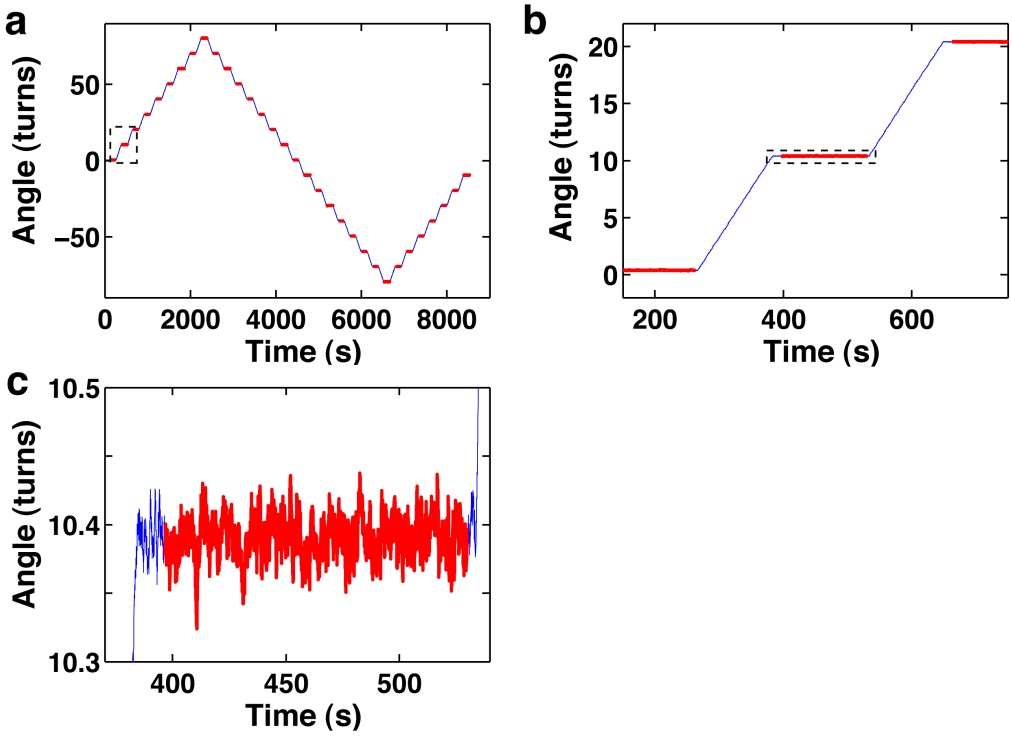

Supplementary Figure 8. Measurement scheme to determine the torsional response of DNA molecules upon over- and underwinding. (a) Angular fluctuations are recorded for a fixed magnet position for $\geq$ 100 s. Then the magnets are rotated for ΔN full turns and angular fluctuations are again recorded at fixed magnet positions. This process is repeated several times. Angular recordings at fixed magnet positions are the plateaus in the angle vs. time trace. The sections of the plateaus highlighted in red are used to determine the mean and standard deviation at the given number of turns N. This information is used to determine the torsional response of the tethered molecule (see main text). The sloped regions in the angle vs. time trace correspond to the instances where the bead rotates in synchrony with the magnets. For the trace shown, the DNA is first overwound in a stepwise manner ($|\Delta N|$=10 turns for all steps) up to N=80 turns, then the rotation direction is reversed until the DNA is underwound up to N=-80 turns, and finally the rotation direction is reversed again. (b) A close-up of the region highlighted by the dashed rectangle in (A), comprising the first three plateaus. (c) A close up of the region highlighted by the dashed rectangle in (B), zooming in on one plateau. The beginning and end of each plateau are excluded from the analysis (see range of red highlighting) of the mean and standard deviation to avoid any biases due to equilibration of the bead after rotating the magnets.

Nature Methods: doi:10.1038/nmeth.1520

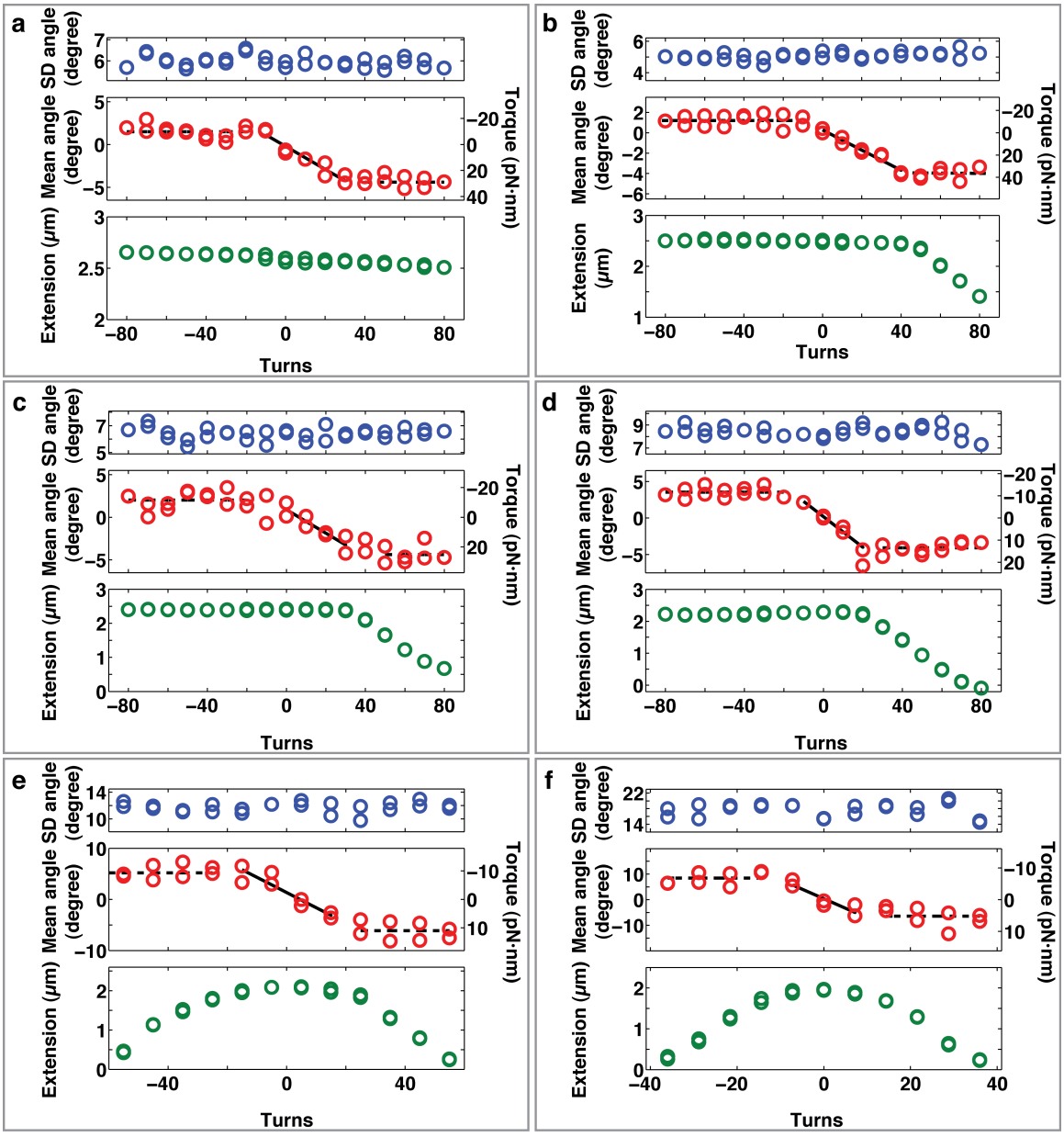

Supplementary Figure 9. Torque measurements for dsDNA at varying stretching forces. Panels (a)-(f) show data for a stretching force of 6.5, 3.5, 2, 1.1, 0.5, and 0.25 pN, respectively. At each force, twist curves similar to Supplementary Fig. 8a were recorded at the different stretching forces. From the twist curves, the mean and standard deviation of the angular fluctuations and the tether extension were determined as a function of the number

Nature Methods: doi:10.1038/nmeth.1520

of applied turns.

In each panel, the standard deviation of the angular fluctuations, which is directly related to the torsional stiffness of the trap, is shown in the top graph as blue circles. It is apparent that the standard deviation is approximately constant for a given measurement at a particular force. The standard deviation does tend to increase, however, with decreasing stretching force (see also Supplementary Fig. 5). The middle graph in each panel shows the mean of the angular fluctuations as a function of magnet rotation as red circles. The shift in mean angle was converted to a torque measurement using Equation 1 and 2 of the main text; the torque is shown on the right axes in the middle graphs. The solid lines indicate the linear fits from which the torsional stiffness of DNA was determined. The dashed lines at far negative and far positive turns in the middle panels indicate the saturation values of the torques from which the denaturation torque (at negative turns for forces above 1 pN), the critical torque for the transition to P-DNA (at positive turns for the 6.5 pN force data), and the buckling torques were determined. Different fitting ranges are chosen at different forces, which is necessary due to the fact that the buckling points and the number of turns at which the magnetic bead approaches the surface depend on the stretching force. In the bottom graph in each panel the tether extension is plotted as a function of the number of applied turns as green circles. We note that even though the DNA buckles at a lower torque and smaller number of applied turns with decreasing stretching force, the shift in mean angle remains constant or even increases for decreasing force since the torsional trap stiffness decreases (Supplementary Fig. 5). Multiple data points for each number of turns correspond to repeat measurements for the same magnet rotation setting. The data were typically recorded starting at 0 turns, going out to positive turns, scanning to back all the way to maximal negative turns, and returning to 0. All measurements are performed using the 7.9 kbp DNA construct in PBS buffer.

Nature Methods: doi:10.1038/nmeth.1520

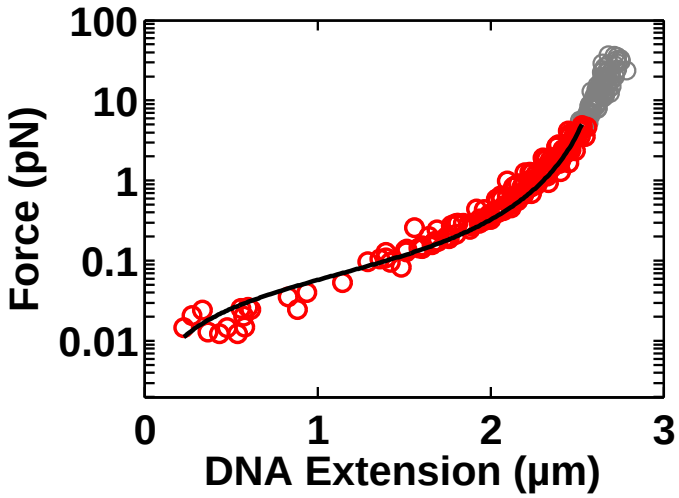

Supplementary Figure 10. Force-extension behavior of double-stranded DNA. The data shown are from ten independent measurements in PBS buffer. Data points in the entropic stretching regime of DNA (< 5 pN, highlighted in red) are well described by the worm-like chain (WLC) model[8–10]. From a fit of the WLC model using the parametrization of Bouchiat *et al.*[11] (black line) to the data in the entropic stretching regime, we find a contour length of $L_c = 2.7 \pm 0.1$ μm, in close agreement with the expected crystallographic length of 2.72 μm for our 8 kbp DNA construct, and a persistence length $L_p = 44 \pm 3$ nm, in good agreement with the results of Wang and coworkers[12] obtained under similar buffer conditions.

Nature Methods: doi:10.1038/nmeth.1520

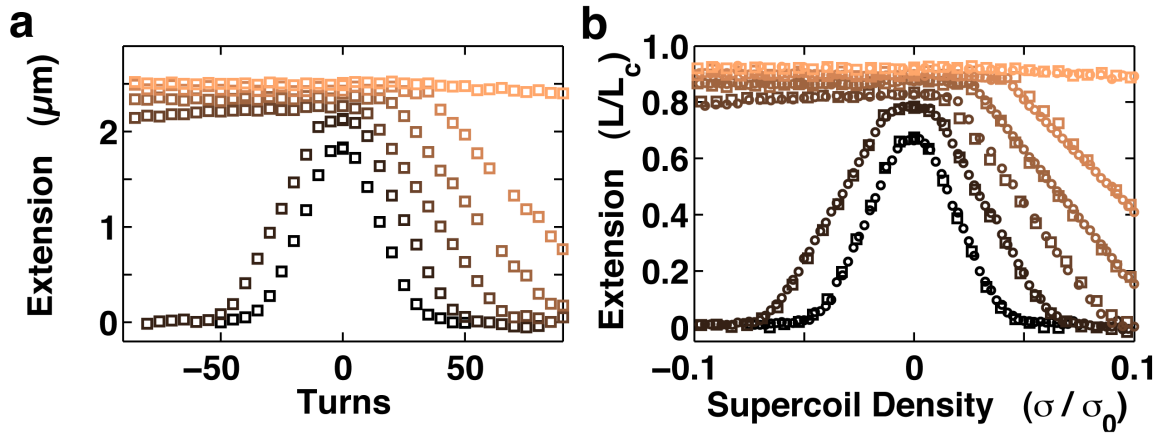

Supplementary Figure 11. Rotation-extension behavior of double-stranded DNA. Representative rotation-extension curves at constant stretching forces are shown for F= 0.25, 0.5, 1.1, 2, 3.5, and 6.5 pN, color coded from dark to light; same color code for both panels. (a) Rotation-extension curves for the 7.9 kbp DNA construct used for all torque measurements in this study. (b) Rotation-extension curves for 7.9 kbp (squares; same data as in (a)) and 20.7 kbp DNA (circles) with the extension rescaled by their contour length L_c (L_c(7.9 kbp) = 2.71 μm; L_c(20.7 kbp) = 7.14 μm) and the number of applied turns converted to supercoil density by dividing the number of applied turns by Lk_0 = (number of bp)/(10.5 bp per turn). The extension-rotation behavior is independent of DNA length after applying the appropriate scaling to both axes.

Nature Methods: doi:10.1038/nmeth.1520

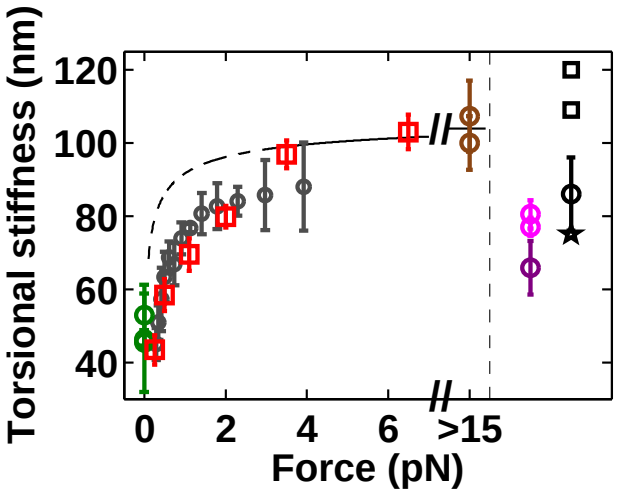

Supplementary Figure 12. Comparison of values for the effective twist persistence length C of DNA as a function of force determined by different methods. Red squares are values of C as a function of force determined in this work from linear fits of the torque vs. applied turns data in the elastic twist regime. As in Fig. 2f of the main text, values for twist persistence length from fluorescence polarization anisotropy measurements of short linear DNA constructs are shown at zero stretching force[13–15] (green circles), and data at stretching forces of 15-45 pN obtained using a rotor bead assay[16] are shown at "> 15 pN" (brown circles). As discussed in the main text, our measurements agree, within experimental errors, with these measurements in the high and zero force limits.

Indirect measurements by thermodynamic integration. Mosconi *et al.* obtained $C(F)$ indirectly using a thermodynamic integration scheme using Maxwell relations[17] from conventional MT data[18] (grey circles). Overall, their data agree with our measurements, in the force range that they have studied, within experimental error. However, closer inspection of their data at the high end of their force range (2-4 pN) reveals that their measurements, even though in agreement within experimental error, tend to fall below the values that we have observed. Consequently, they arrive at a lower estimate of C in the high force limit of 94 ± 7 nm, lower than our measurements of 103 ± 5 nm at F = 6.5 pN and lower than the values of 100 ± 7 nm and 107 ± 10 nm observed by Bryant *et al.*[16] at F = 15-45 pN. Future research will have to show whether these deviations are explained by experimental scatter, are intrinsic to the indirection thermodynamic integration method, or are caused by other experimental differences.

Theoretical model for $C(F)$ by Moroz and Nelson. Moroz and Nelson have proposed a model for DNA in which bending fluctuations reduce the effective torsional modulus, yielding an approximate analytical expression based on an expansion valid in the high force

Nature Methods: doi:10.1038/nmeth.1520

limit[19]:

$$C = C_{\mathrm{lim}} \left(1 + \frac{C_{\mathrm{lim}}}{4L_p} \sqrt{\frac{k_B T}{L_p F}} \right)^{-1} \tag{10}$$

where C_{lim} is the value of C in high force limit. By comparing to the conventional MT data of Strick *et al.*[20] they found[19] $C_{\mathrm{lim}} = 120$ nm and in a later analysis including more data[21] they found $C_{\mathrm{lim}} = 109$ nm (black squares). Comparing to our measurements, their model (with $C_{\mathrm{lim}} = 109$ nm) provides an adequate description at forces above ≈ 2 pN (solid black line), but overestimates the torsional stiffness at lower forces (dashed black line). These deviations are likely at least partially due to the approximations made in the high force expansion used in the Moroz-Nelson model theory. However, they might indicate that additional factors need to be taken into account to obtain quantitative agreement between theory and experiment over the entire force range. We note that measurements at zero or low tension consistently appear to give lower estimation of C than those at high tension. A full exploration of all potentially relevant parameters, such as DNA length, sequence, salt concentration, etc. and the development of a theoretical model that captures these dependences are beyond the scope of this work.

Determination of C from plasmid circularization. Symbols shown on the righthand side of the plot, separated by a vertical dashed line, were obtained by methods that do not control the stretching force or integrate data at different stretching forces. Measurements from topoisomer distributions of circularization experiments on short DNA plasmids have yielded $C \approx 80$ nm, a value that lies between the low and high force limits[15,22,23] (magneta circles), in agreement with the suggestion that circularization of small DNA segments induces strain that acts as an effective stretching force[14,15]. A similar value of $C = 66 \pm 7$ nm was determined from circularization kinetics of DNA plasmids[15,24] (dark purple circle).

Determination of C from theoretical analyses. Theoretical treatments have obtained values for C by comparing to conventional MT results obtained at different forces. Their results of 75 nm (black star[25]) and 86 nm (black circle[26]) are similarly between the low and high forces limits, as might be expected if data at different forces are integrated. The theoretical analysis of Moroz and Nelson that explicitly takes into account the force-dependence of C is discussed above (black squares).

Measurements of C using optical torque tweezers. Forth *et al.*[12] report values of $C = 90 \pm 3$ nm and 88 ± 4 nm from measurements using an optical torque tweezers set up and 2.2 and 4.2 kbp DNA, respectively, however, without reporting the stretching force at which the data were obtained. Similarly, Oroszi *et al.* report values of 73 ± 10 nm and 68 ± 12 nm employing an optical torque tweezers set up[27], also without reporting a clear force calibration. It is an interesting direction of possible future research to directly compare

Nature Methods: doi:10.1038/nmeth.1520

MTT measurements to the results of optical torque tweezers, in particular since the two experimental configurations employ different physical principles.

Nature Methods: doi:10.1038/nmeth.1520

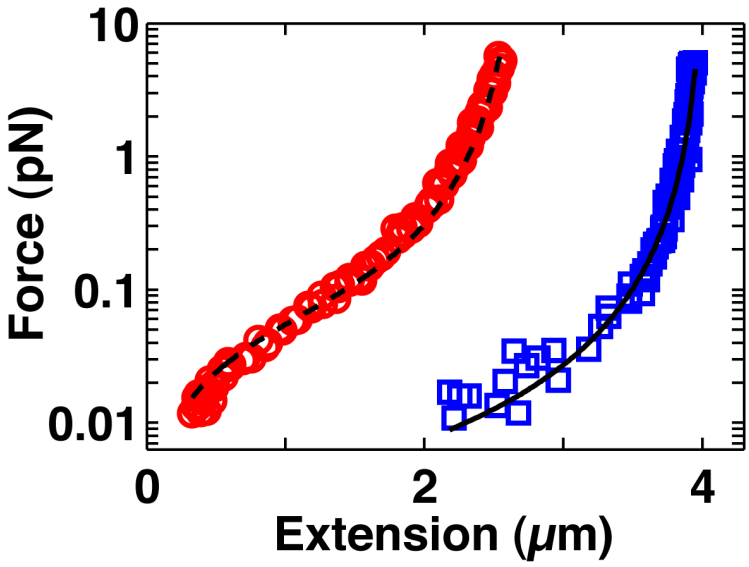

Supplementary Figure 13. Force-extension measurements for RecA-DNA heteroduplex filaments. Magnet tweezers measurements of the force-extension behavior of (torsionally relaxed) dsDNA (red circles) and RecA-dsDNA filaments (blue squares). Fits of the WLC model[11] yield L_c=2.7 ± 0.1 μm and L_p=46 ± 3 nm for bare DNA (dashed black line) and L_c=4.1 ± 0.1 μm and L_p=750 ± 100 nm for the RecA filament (solid black line). The bare DNA measurements were performed in the absence of ATP-γS and RecA, but otherwise in the same buffer as the RecA experiments (see section "Buffer conditions and RecA stocks"). The fitted contour and persistence length for DNA are in good agreement with the expected crystallographic length and with measurements in PBS buffer (Supplementary Fig. 10). The contour length of the RecA filament is increased by a factor of 1.5-fold compared to bare DNA, as expected from the known structure[28] for a fully assembled RecA heteroduplex filament. The fitted persistence length of the RecA filament of L_p=750 ± 100 nm is in agreement, within experimental error, with earlier stretching experiments of Hegner *et al.*[29] and Leger *et al.*[30].

Nature Methods: doi:10.1038/nmeth.1520

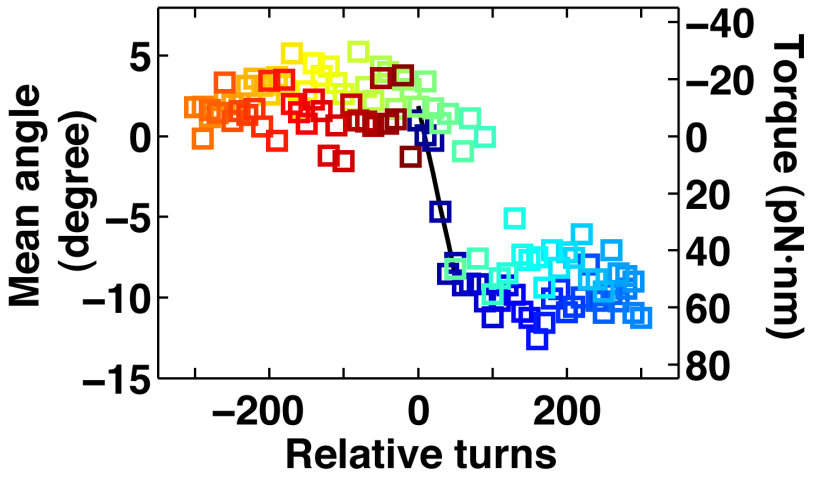

Supplementary Figure 14. Torque response of a RecA filament at $F = 3.5$ pN. Turns are measured with respect to the torsionally relaxed RecA filament, i.e. offset by +330 turns. Data points were recorded in the order indicated by the color code: Starting at 0 relative turns (dark blue), going to 300 turns (light blue), returning to 0 turns (green), going to -300 turns (yellow/orange), and returning again to 0 turns (dark red). The initial slope of the torque vs. applied turns response (black line) gives a torsionally stiffness of 191 nm for this measurement. The torque signal does exhibit some hysteresis (compare the measurements from 0 turns to 300 relative turns to the measurements going from 300 back to 0).

Nature Methods: doi:10.1038/nmeth.1520

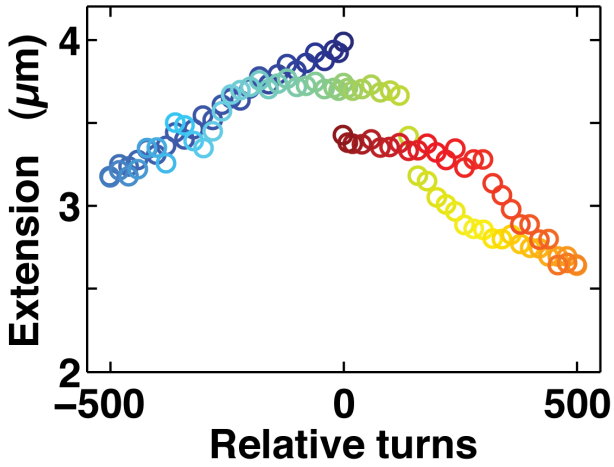

Supplementary Figure 15. Partial disassembly of a RecA filament determined from its rotation-extension response at $F = 3$ pN. Turns are measured with respect to the torsionally relaxed RecA filament, i.e. offset by +330 turns compared bare DNA. Before the start of the experiment, a fully assembled RecA-DNA filament was prepared that gives a stretching and rotation-extension response similar to the traces shown in Fig. 3a,b. Subsequently, unbound RecA and ATP-γS were removed from the flow cell by flushing ten flow cell volumes of RecA assembly buffer without RecA or ATP-γS. The previously assembled filament is initially stable under this buffer exchange: The extension did not significantly change after waiting for 10 (not shown) or 20 min (dark blue data point at 0 relative turns). Finally, a rotation-extension curve was recorded where data points were measured in the order indicated by the color code: Starting at 0 relative turns (dark blue) going to -500 turns (light blue), returning to 0 turns (light green), going to +500 turns (yellow/orange), and returning to 0 turns (dark red).

RecA disassembly and the mechanisms of torsional strain release in RecA filaments. The rotation-extension curves both in the absence and presence (Fig. 3a) of free RecA and ATP-γS show only a modest decrease in length per turn that suggests that the filament does not buckle and that torsional strain is released through other mechanisms. One such mechanism likely involves unbinding of RecA upon over- and underwinding, since the filament returns to its original length if the over- or underwinding is reversed in the presence of free RecA and ATP-γS in solution (Fig. 3a), yet fails to fully recover its length if no rebinding is possible. The observation of partial disassembly, as judged from the reduced length of the filament, after application of positive or negative torsional strain in the absence of free RecA and ATP-γS suggests that both over- and underwinding of the filament are

Nature Methods: doi:10.1038/nmeth.1520

partially accommodated by unbinding of RecA monomers. However, torque-induced RecA dissociation alone cannot account for the release of torsional strain, as this would predict i) a decrease of -4 nm/turn from the geometry of the filament, ii) complete RecA dissociation (and return to the behavior of bare DNA) after overwinding by ∼380 turns, and iii) under conditions in which rebinding is not possible, no (partial) length recovery upon mechanical removal of the torsional strain: predictions which are not borne out by our experiments.

An additional mechanism of torsional strain release is provided by the observation that the maximal torques that RecA-dsDNA can sustain are, within experimental error, identical to the maximal torques that B-form DNA can sustain prior to forming scP-DNA upon overwinding (∼ 40 pN·nm) or prior to denaturing the DNA upon underwinding (∼ -10 pN·nm). The value of the saturation torque of ∼ 40 pN·nm upon overwinding suggests that in addition to RecA dissociation the DNA in the filament is locally converted to the scP-form. This mechanism is supported by the fact that the slope in the extension-rotation curve upon overwinding is ≈ -1 nm/turn, very similar to the slope observed for P-DNA formation in the absence of RecA[31,32] (Supplementary Fig. 11). The similarity of the critical torque upon underwinding the RecA-DNA filament to the denaturation torque of bare DNA suggests that local DNA denaturation in addition to RecA dissociation might be involved in the release of torsional strain. However, the interpretation of the slope of the rotation-extension curves for underwound RecA-DNA filaments is complicated by the fact that RecA is expected to bind single-stranded DNA with high affinity[28,30]. In summary, the filament's increased torsional stiffness does not translate into an ability to sustain increased torques compared to bare B-form DNA. Rather, our measurements indicate that these under- and overwound DNA conformations can exist within the heteroduplex filament and release torsional stress.

Nature Methods: doi:10.1038/nmeth.1520

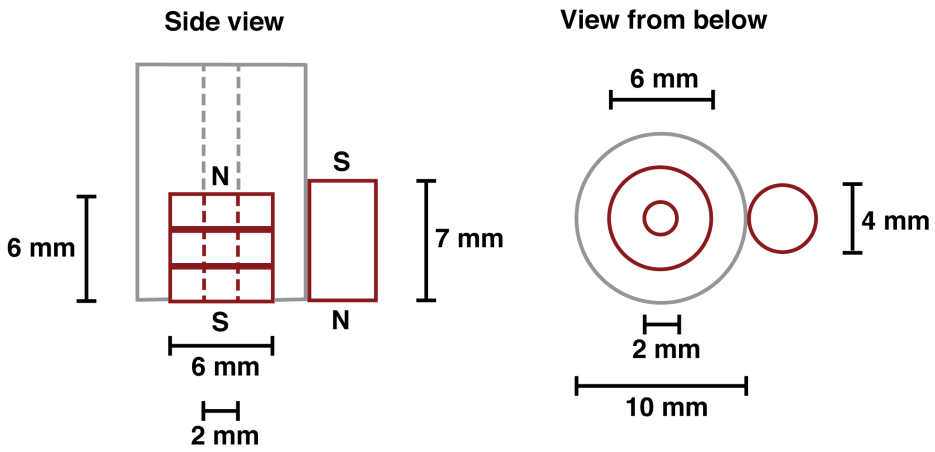

Supplementary Figure 16. Schematic of the magnet assembly for the MTT. The central and side magnet are shown in brown. The magnets are held in place by a custom made magnet holder machined from aluminum, shown schematically in grey. The attachment of the side magnet is facilitated by a small strip of double-sided adhesive tape (not shown).

References

1. Lipfert, J., Hao, X. & Dekker, N. H. Quantitative modeling and optimization of magnetic tweezers. *Biophys. J.* **96**, 5040–5049 (2009).

2. Klaue, D. & Seidel, R. Torsional stiffness of single superparamagnetic microspheres in an external magnetic field. *Phys. Rev. Lett.* **102**, 028302 (2009).

3. Berg, H. C. *Random Walks in Biology* (Princeton University Press, Princeton, New Jersey 08540, USA, 1993).

4. Faxén, H. Der Widerstand gegen die Bewegung einer starren Kugel in einer zähen Flüssigkeit, die zwischen zwei parallelen ebenen Wänden eingeschlossen ist. *Ann. Physik* **373**, 89–119 (1922).

5. Janssen, X. J. A. *Magnetic particle actuation for functional biosensors.* Ph.D. thesis, Eindhoven University of Technology (2009).

6. Svoboda, K. & Block, S. M. Biological applications of optical forces. *Annu Rev Biophys Biomol Struct* **23**, 247–285 (1994).

7. La Porta, A. & Wang, M. D. Optical torque wrench: angular trapping, rotation, and torque detection of quartz microparticles. *Phys. Rev. Lett.* **92**, 190801 (2004).

Nature Methods: doi:10.1038/nmeth.1520

8. Smith, S. B., Finzi, L. & Bustamante, C. Direct mechanical measurements of the elasticity of single DNA molecules by using magnetic beads. *Science* **258**, 1122–1126 (1992).

9. Marko, J. F., Siggia, E. D., Smith, S. & Bustamante, C. Entropic elasticity of λ-phage dna. *Science* **265**, 1599–1600 (1994).

10. Vologodskii, A. Dna extension under the action of an external force. *Macromolecules* **27**, 5623–5625 (1994).

11. Bouchiat, C. *et al.* Estimating the persistence length of a worm-like chain molecule from force-extension measurements. *Biophys. J.* **76**, 409–413 (1999).

12. Forth, S. *et al.* Abrupt buckling transition observed during the plectoneme formation of individual DNA molecules. *Phys. Rev. Lett.* **100**, 148301 (2008).

13. Fujimoto, B. S. & Schurr, J. M. Dependence of the torsional rigidity of DNA on base composition. *Nature* **344**, 175–177 (1990).

14. Selvin, P. R. *et al.* Torsional rigidity of positively and negatively supercoiled DNA. *Science* **255**, 82–85 (1992).

15. Heath, P. J., Clendenning, J. B., Fujimoto, B. S. & Schurr, J. M. Effect of bending strain on the torsion elastic constant of DNA. *J. Mol. Biol.* **260**, 718–730 (1996).

16. Bryant, Z. *et al.* Structural transitions and elasticity from torque measurements on DNA. *Nature* **424**, 338–341 (2003).

17. Zhang, H. & Marko, J. F. Maxwell relations for single-DNA experiments: Monitoring protein binding and double-helix torque with force-extension measurements. *Phys Rev E Stat Nonlin Soft Matter Phys* **77**, 031916 (2008).

18. Mosconi, F., Allemand, J. F., Bensimon, D. & Croquette, V. Measurement of the torque on a single stretched and twisted DNA using magnetic tweezers. *Phys. Rev. Lett.* **102**, 078301 (2009).

19. Moroz, J. D. & Nelson, P. Torsional directed walks, entropic elasticity, and DNA stiffness. *Proc. Natl. Acad. Sci. U.S.A.* **94**, 14418–14422 (1997).

20. Strick, T. R., Allemand, J. F., Bensimon, D., Bensimon, A. & Croquette, V. The elasticity of a single supercoiled DNA molecule. *Science* **271**, 1835–1837 (1996).

21. Moroz, J. D. & Nelson, P. Entropic elasticity of twist-storing polymers. *Macromolecules* **31**, 6333–6347 (1998).

Nature Methods: doi:10.1038/nmeth.1520

22. Shore, D. & Baldwin, R. L. Energetics of DNA twisting. II. Topoisomer analysis. *J. Mol. Biol.* **170**, 983–1007 (1983).

23. Horowitz, D. S. & Wang, J. C. Torsional rigidity of DNA and length dependence of the free energy of DNA supercoiling. *J. Mol. Biol.* **173**, 75–91 (1984).

24. Shore, D. & Baldwin, R. L. Energetics of DNA twisting. I. Relation between twist and cyclization probability. *J. Mol. Biol.* **170**, 957–981 (1983).

25. Vologodskii, A. V. & Marko, J. F. Extension of torsionally stressed DNA by external force. *Biophys. J.* **73**, 123–132 (1997).

26. Bouchiat, C. & Mézard, M. Elasticity model of a supercoiled DNA molecule. *Phys. Rev. Lett.* **80**, 1556–1559 (1998).

27. Oroszi, L., Galajda, P., Kirei, H., Bottka, S. & Ormos, P. Direct measurement of torque in an optical trap and its application to double-strand dna. *Phys. Rev. Lett.* **97**, 058301 (2006).

28. Chen, Z., Yang, H. & Pavletich, N. P. Mechanism of homologous recombination from the RecA-ssDNA/dsDNA structures. *Nature* **453**, 489–484 (2008).

29. Hegner, M., Smith, S. B. & Bustamante, C. Polymerization and mechanical properties of single RecA-DNA filaments. *Proc. Natl. Acad. Sci. U.S.A.* **96**, 10109–10114 (1999).

30. Leger, J. F., Robert, J., Bourdieu, L., Chatenay, D. & Marko, J. F. RecA binding to a single double-stranded DNA molecule: a possible role of DNA conformational fluctuations. *Proc. Natl. Acad. Sci. U.S.A.* **95**, 12295–12299 (1998).

31. Fulconis, R. *et al.* Twisting and untwisting a single DNA molecule covered by RecA protein. *Biophys. J.* **87**, 2552–2563 (2004).

32. Allemand, J. F., Bensimon, D., Lavery, R. & Croquette, V. Stretched and overwound DNA forms a Pauling-like structure with exposed bases. *Proc. Natl. Acad. Sci. U.S.A.* **95**, 14152–14157 (1998).

Nature Methods: doi:10.1038/nmeth.1520